

Supplement of Atmos. Meas. Tech., 12, 5391–5415, 2019
<https://doi.org/10.5194/amt-12-5391-2019-supplement>
© Author(s) 2019. This work is distributed under
the Creative Commons Attribution 4.0 License.



Atmospheric
Measurement
Techniques
Open Access


Supplement of

Quantifying organic matter and functional groups in particulate matter filter samples from the southeastern United States – Part 1: Methods

Alexandra J. Boris et al.

Correspondence to: Ann M. Dillner (amdillner@ucdavis.edu)

The copyright of individual parts of the supplement might differ from the CC BY 4.0 License.

1 Generation of Laboratory Standards: Solutions

The concentrations of pure chemical solutions prepared varied depending on the empirical collection efficiency of each chemical. After collection, some chemicals volatilized over relatively short time scales (hours to days); we weighed these filters three times and analyzed via FT-IR spectrometry within ~24 hours to ensure that weight and FT-IR spectra matched as well as possible (these chemicals are noted as “rapid weigh schedule required” within Table S-1).

Table S-1. Characteristics of solutions used for calibrations, including molar absorptivities (as defined for the functional groups used in previous work) calculated over the entire filter areas.

Chemical Standard	Supplier	Purity	Molar Absorptivities (a.u. cm μmole^{-1})				Rapid Weigh Schedule Needed	Solvent
			C=O	CH	cCOH	aCOH		
1-Docosanol	Aldrich	≥98%	--	1.9	--	23.6	Yes	IPA
4-Nitrocatechol	Alfa Aesar	≥98%	--	0.1	--	32	No	DI
Ammonium Nitrate	Acros Organics	≥99%	--	--	--	--	No	DI
Ammonium Oxalate	Spectrum	≥99%	14.2	--	--	--	No	DI
Ammonium Sulfate	Alfa Aesar	≥99.9%	--	--	--	--	No	DI
D-Alanine	Sigma	≥98%	22.4	5.6	25.3	--	No	DI/IPA
D-(+)-Glucono-Delta-Lactone	Sigma	≥99%	11.9	0.4	--	6.7	Yes	DI
Ethyl Palmitate	Sigma	≥99%	7.08	1.2	--	--	Yes	IPA
D-(+)-Glucose	Sigma	≥99.5%	--	0.4	--	9	No	DI
1,6-Anhydro-β-D-Glucose (Levoglucosan)	Fisher Scientific	≥99%	--	0.6	--	9.2	No	DI
Magnesium Chloride, hexahydrate	Sigma	≥98	--	--	--	--	No	DI
Malonic Acid	Sigma-Aldrich	≥98%	12.9	10	10.8	--	No	DI
Meso-Erythritol	Acros Organics	≥99%	--	0.6	--	7.4	No	DI
Nonadecan-10-one	TCI	≥97%	9.9	1.4	--	--	Yes	IPA/etOH
Oxalic Acid	Aldrich	≥99.999%	10.3	--	12.3	--	Yes	DI
Sodium Oxalate	Alfa Aesar	≥99.5%	19.1	--	--	--	No	DI
Squalene	Aldrich	≥99%	--	1.3	--	--	No	IPA/etOH
Suberic Acid	Aldrich	≥99%	13.9	1.3	7.9	--	No	DI
Succinic Acid	Sigma-Aldrich	≥99%	14	6.4	13.1	--	No	DI
Tannic "Acid"	Acros Organics	≥95%	11.4	0.2	--	6.2	No	DI
Terephthalic Acid	TCI	≥99%	19.1	5.8	13.2	--	No	IPA

2 Generation of Laboratory Standards: Filter Weighing

All laboratory standard filters (47 mm MTL PTFE) were pre- and post-weighed to find the mass of the collected aerosol particles. Filters were stored and transported in plastic Petri slides. Ceramic-tip tweezers were used to handle the filters. Each fresh filter was equilibrated with the air in the balance room by allowing the lid to remain slightly ajar for ~24 hours prior to pre- and post-weighing.

The weigh procedure was as follows. All laboratory standard filters were weighed using an ultramicro balance equipped with a filter weighing kit (Mettler-Toledo, <http://www.mt.com/>) and a triangular filter-weighing pan. Operators wore an elastic grounding wrist band. Prior to weighing, the ultramicro balance was adjusted and tested; a difference of $\leq 0.000010\%$ from the internal standard weight was allowed. The balance was exercised by weighing metal 100 and 300 mg standards weights, followed by three “control” MTL 47 mm PTFE filters. The third “control” filter was weighed until three measurements within 2 μg were reached. Each laboratory standard filter was passed near an ionizing strip (Haug Static Control Products, <http://www.haug-static.com/>) for 10-20 seconds, ensuring that all surfaces of the filter were placed near the ionizing strip. The filter was then passed near ^{210}Po alpha ionizer strips (Mettler-Toledo, <http://www.mt.com/>) for 10-20 seconds. Each filter was allowed to equilibrate on the weigh pan with the door open before closing and waiting for the balance measurement to stabilize. The median of at least three replicate weights (measured on three separate days/times) was recorded. We excluded weights exceeding the 95% confidence interval of typical measurements (6 μg).

3 Generation of Laboratory Standards: Filter Standard Collection Procedure

Tweezers were used when handling filters in the lab. Each filter holder set and screen was cleaned with ethanol and deionized water, then dried completely prior to use. The Partisol aerosol sampler was loaded by placing a filter tightly into a holder (Figure S-1), then placing each holder in a stack into a magazine (columns shown inside the sampler in Figure S-2).

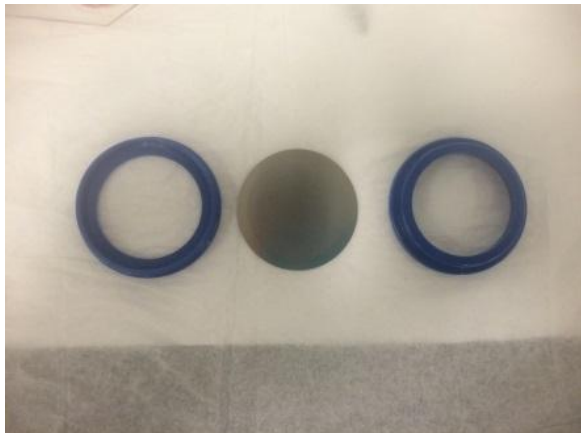


Figure S-1. Partisol filter holder (two outer pieces, between which the screen is sandwiched).



Figure S-2. Partisol Plus 2025 instrument, showing two clear filter magazines within the hollow section of the sampler.

The aerosol generation system was cleaned before collection of each chemical: the system, including all tubing and fittings (Figure S-3), was disassembled and rinsed thoroughly with water and ethanol. If chamber blank filters collected immediately after the deep clean contained material visible in the infrared spectra, the aerosol generation system was re-cleaned. The diffusion dryer was filled with silica desiccant beads that were heat-regenerated after every two to three chemicals were collected (approximately once per month). The aerosol sampler was flushed with DI water or IPA (depending on the solution of pure chemical) for two hours after each deep cleaning procedure, and at least 20 minutes before and after each pure chemical standard collection to avoid buildup of chemical inside the system (typically, several standard filters were collected at a time). Each pure chemical solution was allowed to equilibrate in the aerosol generation system for at least 20 minutes prior to collection of standard filters.



Figure S-3. Sampler setup including atomizer and diffusion dryer in the left hood, and Partisol Plus 2025 sampler in the right hood.

4 Generation of Laboratory Standards: Molecular Environment Considerations

Hydrogen bonding is an influential type of interaction for infrared absorption spectrometry, and can be variable for different preparations of the same chemical. In particular, the carboxylic O-H and alcohol O-H absorption bands were found to differ between the literature spectra and some of those collected in our work, especially when a molecule contained multiple polar, oxygenated functional groups (e.g., oxo-acid or hydroxy-acid). The following paragraphs list chemicals collected as laboratory standards, but not used in the calibration models due to unstable or unclear hydrogen bonding patterns. Behavior of the chemicals within various preparation conditions such as solvent and pH, which were examined in an effort to collect the chemical with a stable and predictable spectrum, are discussed.

The spectrum of racemic tartaric acid contained one or both of two structures, which were presumed to be hydrogen bonding motifs, based on spectral interpretation and comparison with literature spectra (Figure S-4).

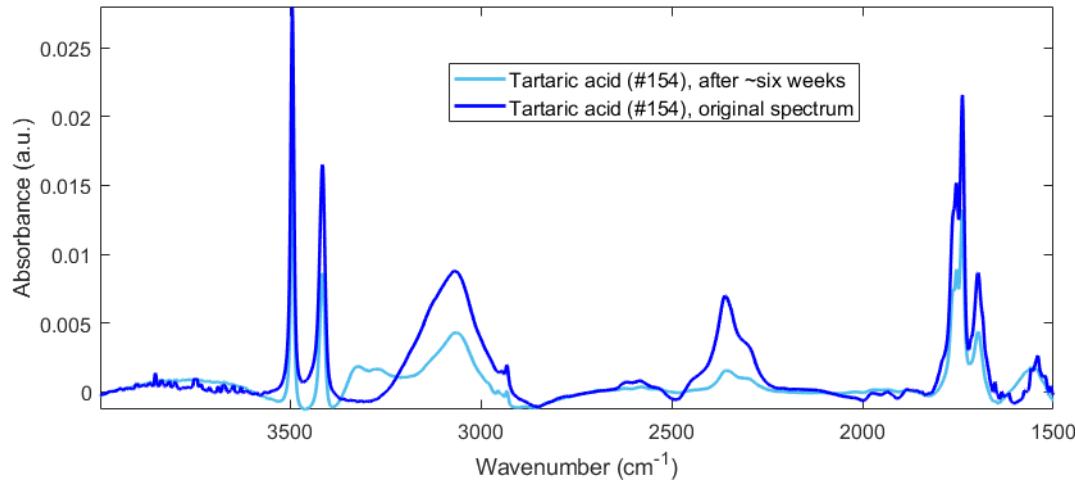


Figure S-4. Spectra of the same tartaric acid particles, just after collection (orange) and ~six weeks after collection (blue). Note the absorption peaks at ~3400-3200 cm⁻¹ in the blue spectrum, possibly indicative of a more stable hydrogen bonding organization. Spectra are baseline corrected.

These included: (1) a conformer with free alcohol O-H stretching peaks at approximately 3500 and 3400 cm⁻¹, a C=O stretching peak with multiple shoulders ~1800-1650 m⁻¹, and a broad hydrogen-bonded carboxylic O-H stretching peak at approximately 3050 cm⁻¹; and (2) a conformer with two broad hydrogen-bonded O-H stretching peaks at approximately 3350 and 3250 cm⁻¹, but no observable C=O or carboxylic O-H stretching peaks. The free (non-hydrogen-bonded) O-H stretching peaks in the former conformer were identified in reference spectra of tartaric acid as well as other alcohol species (e.g., phenolic standards; Bahadur et al., 2010). However, it is unclear which of these alcohol O-H conformers exist in ambient particulate matter samples. The preparation of a tartaric acid solution in water caused a shift from the more carboxylic acid type motif to one with less carboxylic and free alcohol O-H, and more bound alcohol O-H character. Solutions with low pH (~pH 2, adjusted with HCl) and in ethanol were also prepared, and appeared to cause less shift of the hydrogen bonding motif over time toward the bound alcohol O-H character motif. Overall, however, we decided to remove this chemical from the calibration models due to the instability of the spectra and difference from reference spectra.

A set of pyruvic acid laboratory standards were also collected, but not used in our models. Pyruvic acid is known to chemically hydrate to form a gem diol at its ketone functional group, changing the infrared absorption spectrum substantially (Maroń et al., 2011). Differences between our spectra (of crystalline particles) and those in the literature did not allow us to determine whether we had collected exclusively dehydrated pyruvic acid. Therefore, the moles of the alcohol O-H (aCOH) and carboxylic acid (COOH) functional groups were not known based on mass of pyruvic acid collected. Absorption in the same range as the broad OH stretching bands of other alcohol spectra indicated that the ambiguous absorption in the ~3600-3450 cm⁻¹ range was not hydrogen bonded carboxylic acid bending or overtones, but alcohol O-H stretching. Since quantifying the moles of functional group is essential to our model structure, we excluded pyruvic acid from our models.

While *cis*-pinonic acid was successfully collected after testing different concentrations and solvents, the absorption bands present in the spectra varied between days of sampling, and over time. It is likely that the hydrogen bonding motif of *cis*-pinonic acid varied depending on solution concentration, mass of material deposited onto the filters, and other parameters, and that the most energetically favorable hydrogen bonding motif was the end-point for most lab standards, after some equilibration time (Davey et al., 2006). Additionally, the final spectra of many *cis*-pinonic acid standards collected contained strongly negative absorption bands, which we hypothesize to have originated from the Christiansen Effect (Chalmers, 2002). For these various reasons, *cis*-pinonic acid was not used in our calibrations. However, other members of our extended research group have successfully and reproducibly collected *cis*-pinonic acid spectra when using a different type of PTFE filter and aerosol collection system (Takahama et al., 2013).

5 Generation of Laboratory Standards: Volatility and Stability Considerations

Divanillin, an aromatic species with two aldehyde groups, was also collected. However, the solubility in water and IPA was too low, and collected masses were well below the maximum for C=O functional groups used in the

models (Section 2.5 in the main text). In the future, aldehydes such as this should be explored as possible contributors to OM concentrations. The observation of both aldehyde H-C=O stretching peaks in the ~2700-2850 cm⁻¹ range and the presence of a strong C=O stretching band (~1680 cm⁻¹) suggested that the molecules collected were not chemically hydrated to gem-diol form. However, this molecule does contain O-H groups, and the absence of hydrated aldehyde groups could therefore not be ruled out. The spectra of the collected standards suggested, however, that it might be possible to collect other aldehyde species standards in the future. Literature values of hydration constants (Solomons and Fryhle, 2004) also see the work done in Takahama et al., 2013) could guide the selection of a pure chemical.

Levulinic acid, or 4-oxo-pentanoic acid, was selected as a possible oxo-/keto-acid for our calibration. However, this chemical is difficult to handle (it is light sensitive, highly toxic, and has a melting point just below room temperature). We could not collect any material from the solutions prepared of this chemical, despite numerous attempts made by varying the solvent and concentration. It was suspected that the chemical was too volatile for collection as particles.

An acid anhydride was initially a high priority chemical on our list, but after testing both a straight-chain and cyclic example of an anhydride, we chose to leave this sub-category of organic molecules out of our calibration. The two chemicals we tested in this category were palmitic anhydride and naphthalic anhydride. Neither of these two chemicals went into solution at the concentrations we anticipated needing, including with pH adjustment, and we were unable to collect any material onto filters from emulsions. Although it was suspected that the acids or esters would be formed in solution, since no material was collected from these standard solutions (Barros et al., 2001), this hypothesis could not be tested.

6 Generation of Laboratory Standards: Influence of Humidity and Particle Water

Laboratory standards of several chemicals were exposed to wet and dry environments, then analyzed via FT-IR spectrometry to determine the impact of humid and dry environments on the spectra and standards. Filters that were used in calibration were re-used for this study; chemicals selected for examination included hygroscopic species such as glucose, ammonium sulfate, and pyruvic acid (the latter can become a gem-diol in the presence of water; Maroń et al., 2011). Squalene (hydrophobic) and laboratory blanks were also tested as controls. Each filter was analyzed via FT-IR spectrometry and weighed, then exposed to a particular dry/humid environment for one week, and re-analyzed. The filter was then exposed to the opposite environment for one week, and analyzed one final time. Filters were equilibrated with the weigh lab air (Petri slides were left ajar) prior to weighing in order to obtain stable measurements.

Exposing the samples to a dry environment had little to no impact on the observed spectra. This paralleled exposure of the filters to the low humidity environment in the sample chamber of the FT-IR spectrometer. The effect of exposing laboratory standards to a humid environment was a lower FT-IR spectrum absorbance for hygroscopic materials, such as glucose and pyruvic acid. This was hypothesized to be a redistribution of hygroscopic material away from the center of the filters, and out of the path of the infrared beam. The hypothesis of redistribution was

confirmed by the exposure of humidified filters to a dry desiccator. The spectra remained the same after drying, indicating that the mechanism that decreased the spectral absorbance was not reversible.

Hydrophobic species such as squalene and a blank filter were not affected, other than an increase in surrounding water vapor. No chemical changes, such as hydration of carbonyl type functional groups, were observed Figure S-5. It is therefore not anticipated that ambient sample spectra would be chemically different from those of laboratory standards due to the relative humidity of the particles during collection, handling, storage, etc.

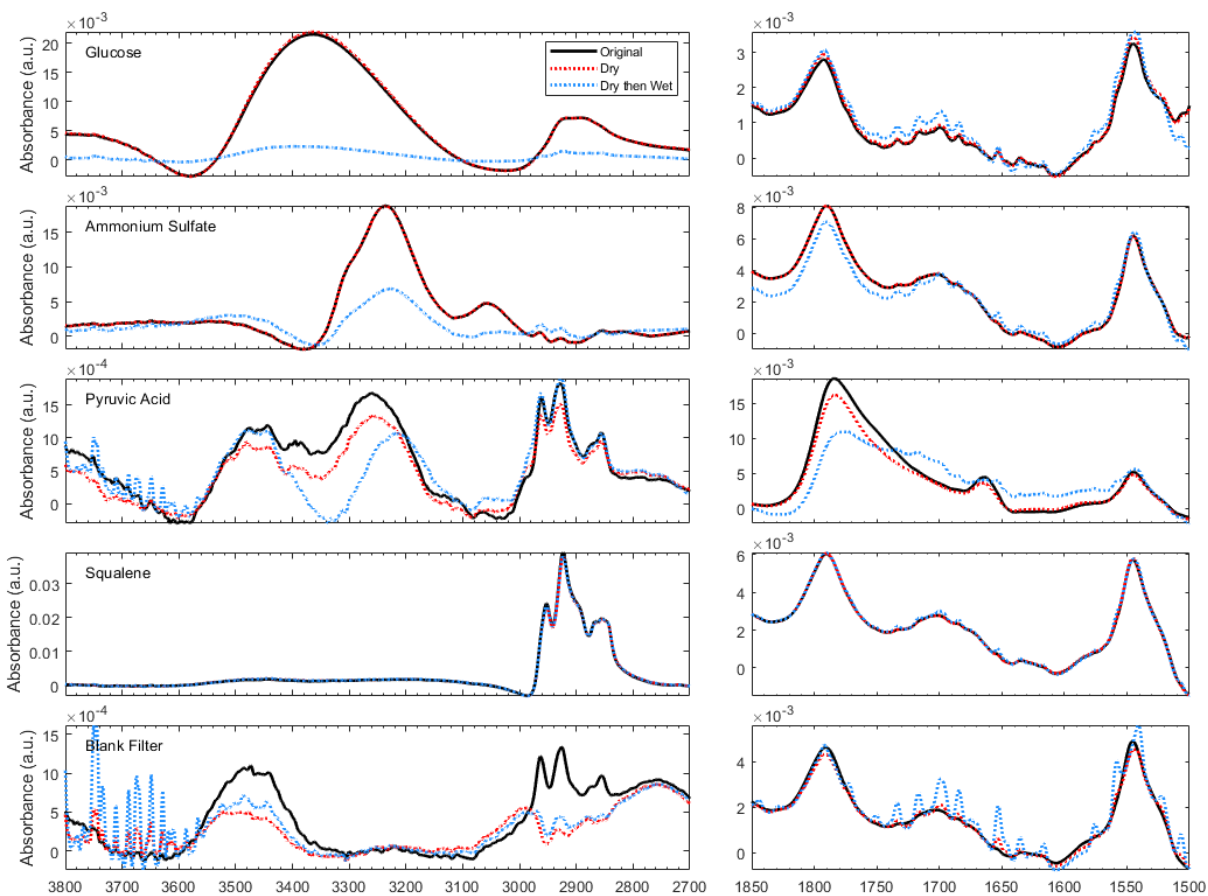


Figure S-5. Spectra collected during testing of humidity exposure impact on laboratory standard filters. A pre-study spectrum, a spectrum after exposure to a dry desiccator (one week), and a spectrum after exposure to a wet desiccator the following week are plotted for each chemical. Results of the opposite exposure cycle were similar.

Particle water absorbs in two mid-infrared spectral regions of interest: a strong, broad band at ~3450-3200 cm⁻¹ corresponds to O-H stretching vibrations, and a weaker, broad band at ~1640 cm⁻¹ corresponds to an H-O-H bending vibration (Mayo et al., 2003). The higher frequency of these absorption bands overlaps spectrally with those of alcohol O-H and N-H stretching. The lower frequency water absorption band overlaps with C=O groups of the oxalates and the amino acid, as well as the conjugated C=C of tannic acid in our laboratory standard spectra. The inclusion of particle water in the models was therefore important to avoid attributing its absorption as functional group material. As in previous work (Cziczo and Abbatt, 2000; Frossard and Russell, 2012), the highly hygroscopic

inorganic salt MgCl₂ was used as an infrared transparent carrier of particle water. Although NaCl was tested as a possible salt for this purpose, MgCl₂ carried more particle water at reasonable collected masses in the low humidity FT-IR spectrometer sample chamber. Seven particle water (MgCl₂) standards were added to all models, as in all other chemicals included, with masses collected ~20-300 µg. Although these were well below theoretical calculations of the particle bound water on aerosol particles in the SEARCH network (Dabek-Zlotorzynska et al., 2011), the intensity of a possible particle water O-H stretching band in the ambient SEARCH sample spectra was used as a constraint for particle water standard collection.

The result of including the particle water standards in the models was most prominent in the aCOH model, as demonstrated by the lower aCOH concentrations measured when particle water was not included (the coefficient of determination, R^2 , of the scatter plot of y =without particle water versus x =with particle water standards included, was $R^2=0.95$ for aCOH; Figure S-6). For the other reported functional groups, $R^2\geq0.99$. Predicted concentrations of functional groups and of OM were unchanged, however (within collocated sampling uncertainties), as indicated by the slopes and intercepts of the comparison scatter plots (Figure S-6).

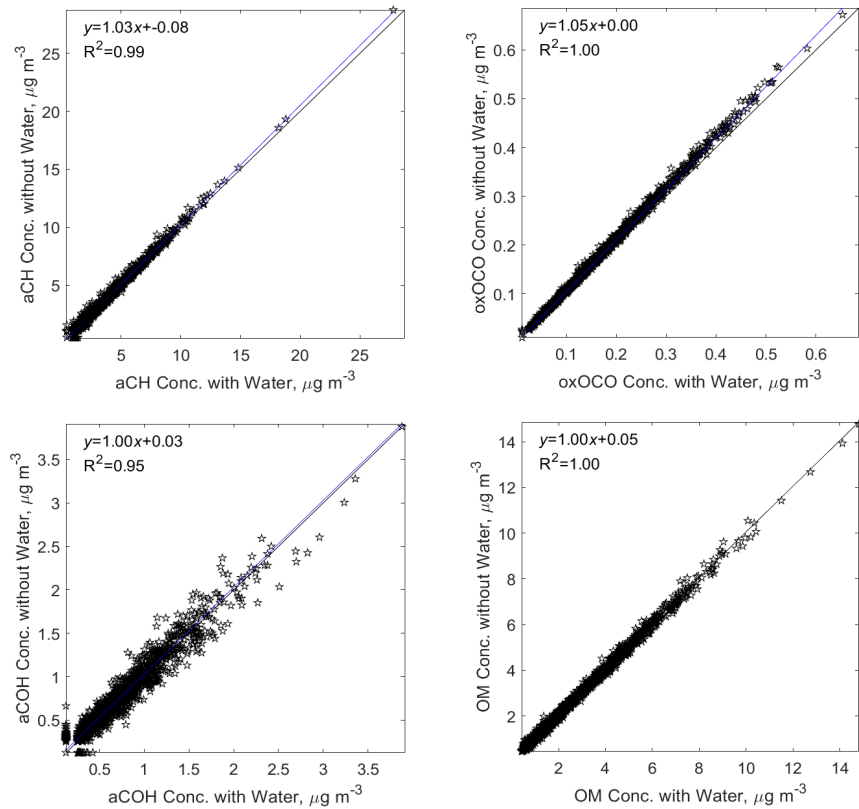


Figure S-6. Scatter plots of several measured functional group and OM concentrations, without (y-axis) versus with (x-axis) including particle water standards in the models. Fitted regressions (blue) are by orthogonal least squares. Oxalates are abbreviated as oxOCO. The black line represents a one-to-one line.

In agreement with these findings, the similarity of re-analyzed to original spectra (main text Section 2.3) was improved when particle water standards were included, due to an increased correlation between aCOH concentrations. The variable importance in the projection (VIP) scores were calculated for the total OM (as discussed in the main text, Section 3.3.1) when particle water standards were not included in the model (Figure S-7).

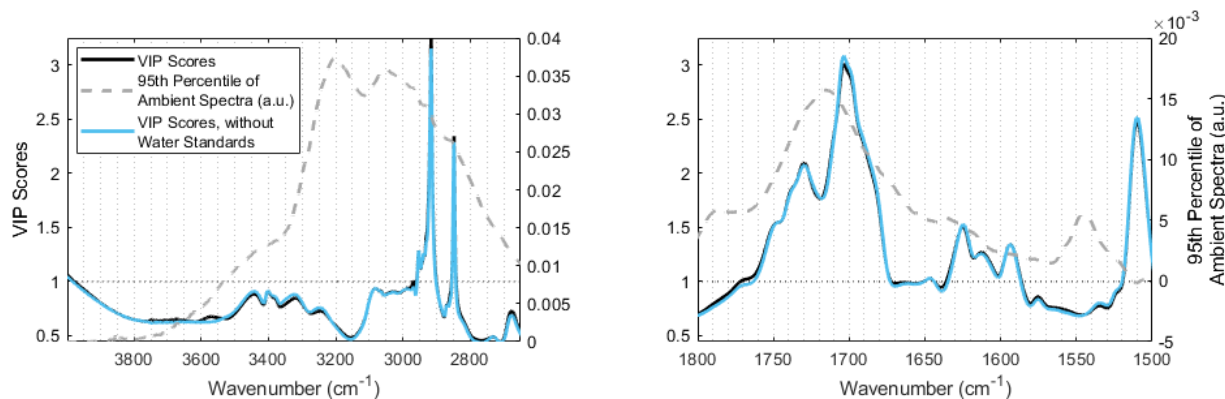


Figure S-7. VIP scores of models with and without particle water standards included.

The comparison of VIP scores demonstrated that, while most predictive features were similar between the models when water standards were not included, some O-H stretching absorption ($\sim 3550 \text{ cm}^{-1}$) was not captured by the models. This suggests that including the water standards allowed the models to determine the contribution of aCOH stretching in this spectral region. The scatter in the plot of compared aCOH predictions in Figure S-6 also suggests that variability between samples was captured differently when water standards were included.

7 Generation of Laboratory Standards: Influence of Mixing Chemicals

The laboratory standards generated in the present study, and used to quantify organic functional groups, contained only one chemical per filter. However, ambient aerosol contains many chemicals, which likely interact. Therefore, although only qualitative collection was possible for multiple chemicals on a single filter due to volatilization and collection uncertainties, multi-component laboratory standards were generated from solutions containing multiple chemicals (Figure S-8).

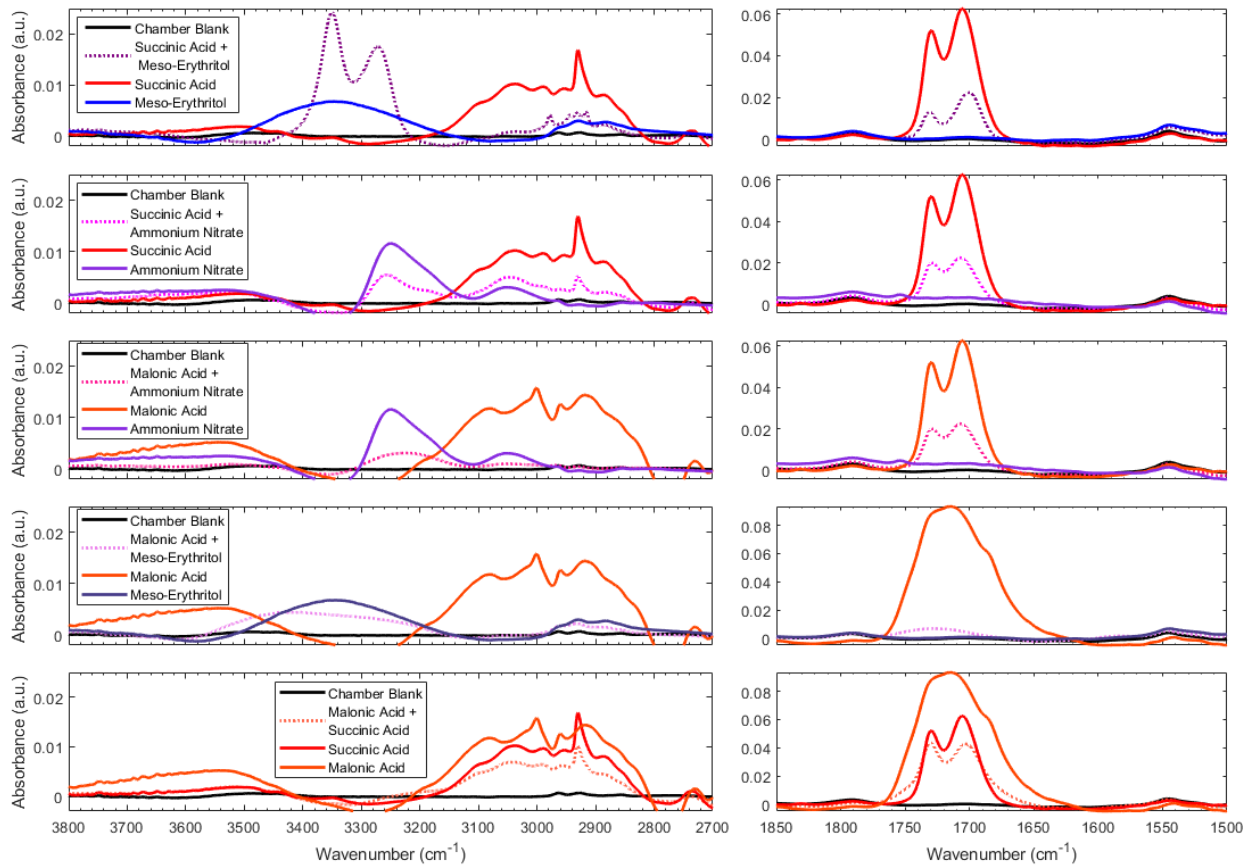


Figure S-8. Spectra of particles collected from mixtures within solution.

Only two major differences from the simple “overlay” of the mixed spectra were observed. First, in the top panel, the O-H stretching band of *meso*-erythritol was split into two peaks in the presence of succinic acid, likely due to the presence of two bonding environments for the *meso*-erythritol alcohol OH groups. Such a change demonstrated that the two chemicals interacted within the collected aerosol particles. Similarly, the O-H stretching band of *meso*-erythritol was broadened and shifted in the presence of malonic acid (second plot from the bottom). Perhaps two bonding environments of the *meso*-erythritol O-H groups are again present, and simply appear as a broadened peak in the mixture spectrum. Clearly, again, these spectra demonstrated that the molecules within the organic aerosol particles interacted through hydrogen bonding, impacting observed infrared absorption. No changes in C=O stretching frequency were observed in any of the multi-component standards. Note that absorbances below the x-axis are negative due only to baseline correction. Overall, the changes in spectra due to mixing of chemicals could result in added scatter to, or over- or under-estimation of, functional group concentrations. Added scatter in predictions could result from regression coefficients not capturing true variance at the frequencies where bonds are absorbing in real aerosol samples. Over/under-estimation of functional group concentrations would result if the regression coefficients mis-attributed spectral features. The consistency of the C=O stretching band absorption features in pure and mixed standards suggests that some functional groups would be only slightly impacted, if at all.

Multi-component standards were also collected using another, sequential method of collection: one chemical was collected onto a filter, weighed, analyzed via FT-IR spectrometry, and a second chemical was collected, etc. Both methods generally provided similar results. The mixture of terephthalic acid with levoglucosan did demonstrate a slight shift in the C=O absorption region of the acid (1696 to 1692 cm⁻¹); further work on multi-component standards should explore this or similar interactions. The in-solution mixture standards are overall likely to be more similar to the internally mixed aerosol particles from the humid Southeastern US atmosphere, so were reported here.

8 Model Factor Selection

Selection of the number of factors can influence the model results strongly, so care was taken to find a method for selecting the most appropriate number for our models. Methods tested include the root mean squared error of cross validation (RMSECV; Naes et al., 2002), selection of a local minimum within the RMSECV surface (Li et al., 2002), modified RMSECV (van der Voet, 1994), root mean squared error of calibration (RMSEC), root mean squared error of prediction (RMSEP), a custom bias/error inclusion metric from Takahama and coworkers (Takahama and Dillner, 2015), explained variance in the test set of standard functional group moles, and simulated annealing (SA; Ledesma et al., 2012). Ultimately, the number of PLS factors should be selected using the minimum RMSECV, so that the values were allowed to vary in each model version.

9 Model Dynamic Range

In contrast to a typical analytical calibration (e.g., for chromatography), multiple chemicals were included in each functional group calibration model in the present work. We necessarily asked the question, then, whether we should include a dynamic range of each specific chemical within the plausible range for that particular chemical, or for the functional group in total. The responses of chemical standards were clearly linear in FT-IR spectrometry (the molar absorptivities are listed in Section 1 of this Supplementary Material), indicating that the moles of functional group could be predicted accurately, given even the inclusion of only low calibration points. However, the PLS algorithm derived regression coefficients from maximal covariance in spectra and weighed quantities, such that the moles of each chemical included in the calibration impacted the regression coefficients. We therefore designed our functional group calibration models within the dynamic range of the *total* functional group moles estimated to be present in ambient samples.

A SA analysis was used in selecting the maximum number of moles of functional groups in each model. SA selected the number of factors based on the ambient sample predictions by finding the minimum of an error function (rather than by optimizing a model error metric that was based on the laboratory standards). The SA algorithm operated by adding random, small values (e.g., 1-5) to the maximum number of moles included in each functional group model (as an array). The models were then limited to the laboratory standards with collected functional group moles less than or equal to the maximum number of moles in each SA randomized array. The PLS regression algorithm was performed using those standards, and the model result with the minimum sample RMSEP (between the predicted and TOR OC concentrations for the test set of ambient samples) was selected. The maximum number of moles of

three of the four functional groups were optimized simultaneously and reproducibly using this method. The fourth functional group, COOH, was included in the simulated annealing, but because its functional group/C atom ratio was assumed to be zero (all C atoms in the carboxylic acid group were initially accounted for by C=O), this value was instead determined based solely on logistical factors such as collection efficiency of chemicals. The resulting maximum numbers of functional group moles included in the calibration models were adjusted slightly to allow an acceptable number of standards (seven) for each chemical to be included in the models, considering logistics of laboratory standards collection.

10 Model Construction: PLS Calibration and Pre-Processing

The conceptual framework for construction of our functional group models is demonstrated in Figure S-9. The absorption bands of the laboratory standard spectra (upper subplot) overlap with those in the ambient sample and field blank (lower subplot) such that features from the laboratory standard spectra are used in the PLS regression to quantify the functional group material. Each functional group model is constructed by finding the maximal covariance between the absorbance and functional group moles in the laboratory standards. No information from the ambient sample spectra is used to build the models. The chemicals included in the model are found in the atmosphere and/or represent chemicals that are present in the atmosphere, so that the spectra can be used to approximate the ambient spectra.

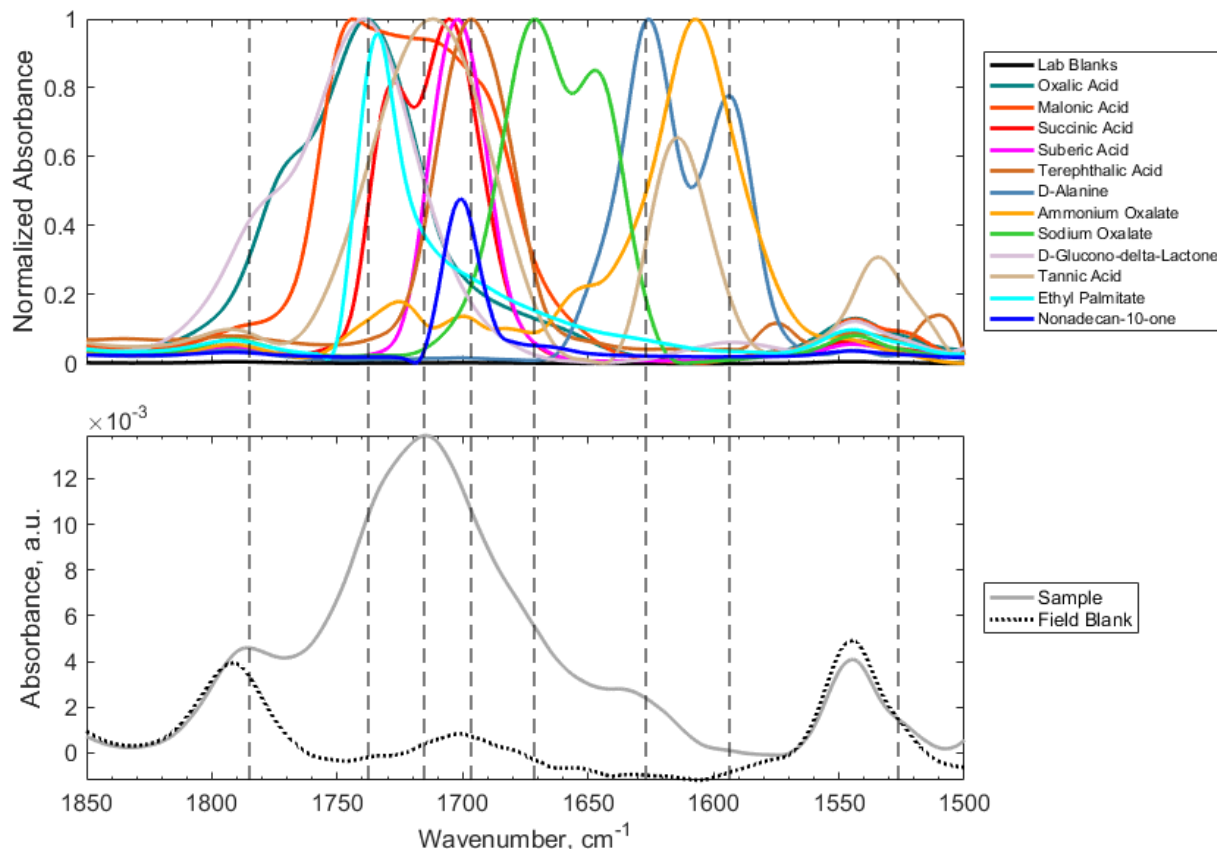


Figure S-9. Stacked, normalized spectra subplots with (a) standards on top and (b) sample and field blank on bottom. Demonstrates how our method works, where all these different carbonyl species fit in. Zoomed to carbonyl stretching region.

It is possible to construct models for multiple functional groups simultaneously using an algorithm called PLS2 (Andersson, 2009). Although this would have been theoretically concise, the method was, in practice, complicated and gave poor results for our dataset. For example, since C-H bonds were present and abundant in most chemical standards, they were weighted too heavily. This generated predicted OM concentrations that were much lower than anticipated (~27% of calculated residual OM), and OC estimates that were higher than probable given that FT-IR “sees” only the majority of C bonds (100% of TOR OC).

The final models reported in this work include only wavenumbers above 1500 cm^{-1} , while we actually collected to 420 cm^{-1} . The decision to truncate was made after examining the regression coefficients and predictions from using the full spectra. Since the range between 4000 and 1500 cm^{-1} includes overtone absorption bands from PTFE (Liang and Krimm, 1996) that are similar in size to the aerosol absorption bands, there was no need to include the lower end of the spectral range (which would also have informed the models about PTFE variations). The aerosol absorption features below 1500 cm^{-1} in our laboratory standards were mostly specific to each molecule (rather than across a functional group), and the very strong absorption of PTFE in the $1400\text{-}1200\text{ cm}^{-1}$ range decreased the variance captured by our regression coefficients for the actual aerosol material.

Pre-processing including derivatives and baseline correction were also tested for our models. However, using the raw spectra resulted in more interpretable regression coefficients and better prediction power of our models relative to TOR OC concentrations and residual OM concentrations.

11 Model Construction: Partitioned Functional Groups

Calibration models for eight functional groups were constructed, although not all were reported, and those functional groups were measured within the ambient samples. Following this measurement, one additional functional group was estimated from the relationships of the functional groups that were obtained by calibration: non-acid, non-oxalate carbonyl (naCO).

The naCO was estimated following the method of Takahama and coworkers (2013). The measured COOH functional group moles were regressed against the moles of non-oxalate carbonyl (noxCO; Figure S-10). If the difference between the moles for a given ambient sample of COOH and non-oxalate carbonyl (noxCO) was within 5% (if they were approximately equal), moles of naCO were assumed to be zero. If the difference between the moles for a given ambient sample of COOH and noxCO was more than 5% (if there was excess non-acid carbonyl), moles of naCO were assumed to be the difference between noxCO and COOH. If these two conditions were not met, the moles naCO moles were assumed to be zero. Figure S-10 demonstrates the relationship between the COOH and naCO moles measured.

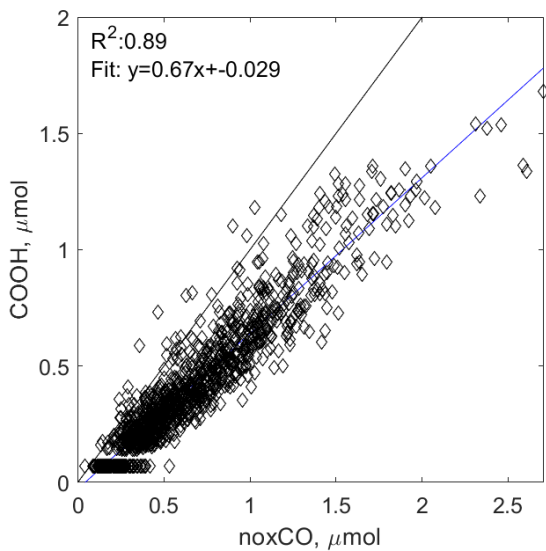


Figure S-10. Regression of measured COOH and noxCO moles used in estimating moles of naCO functional group. The blue line represents the orthogonal least squares regression fit, while the black line represents a one-to-one line.

A regression was also made between the two calibrated types of CH bonds (aliphatic C-H or CH and unsCH), summed, and the calibrated total CH bonds (Figure S-11). The result demonstrated that the summed unsCH and aCH moles were slightly, but consistently greater than the total CH moles. This was likely due to the information added when separating the two types of bonds, increasing the overall measured moles of CH.

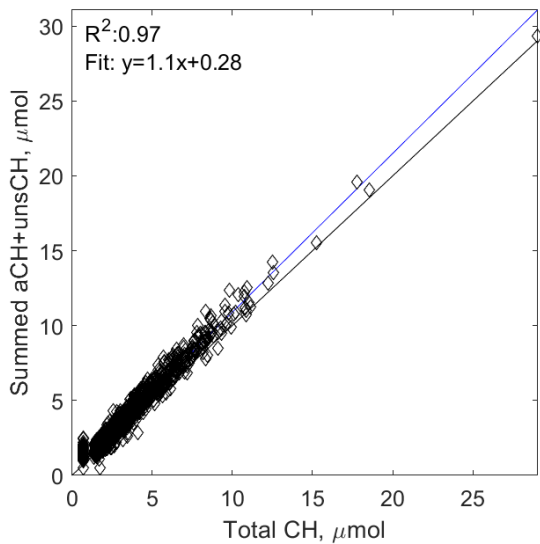


Figure S-11. Regression of measured saturated and unsaturated CH (aCH and unsCH, respectively) with total CH moles. The blue line represents the orthogonal least squares regression fit, while the black line represents a one-to-one line.

Similarly, the summed molar contributions of different C=O containing functional groups were regressed against the calibrated total C=O moles (Figure S- 12). The results in this case demonstrated a slight underestimate of the total C=O. Perhaps this indicates that additional C=O containing standards are needed in the models to fully capture the variance of C=O.

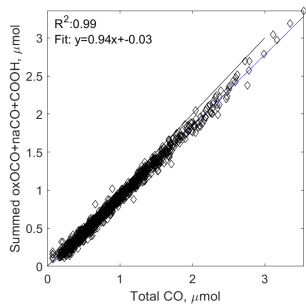


Figure S-12. Regression of measured contributors to the total carbonyl moles (oxOCO, naCO, and COOH) with the total moles of carbonyl (CO). The blue line represents the orthogonal least squares regression fit, while the black line represents a one-to-one line.

12 Model Interpretation: Variable Importance for the Projection Scores

The VIP scores were calculated to simplify interpretation of our models. The following equation for VIP scores of the total predicted FT-IR OM was derived, based on the equation presented in Weakley et al., 2016 and work of Chong and Jun, 2005.

$$VIP_j = \sum_g \sqrt{\frac{p_g \frac{\lambda_g^2}{\lambda_{OM}^2} \sum_{a=1}^A EV(\%)_{y,a,g} w_{a,j,g}^2}{\sum_{a=1}^A EV(\%)_{y,a,g}}} \quad \text{Equation 1}$$

In Equation 1, p is the number of wavenumbers/predictor variables included in our spectra, λ_g values are the weights of mass OM per mole functional group for each functional group and for all functional groups, summed (λ_{OM}), λ_g / λ_{OM} thus gives the fraction of lambda for each functional group), A is the number of factors selected for the calibration model of functional group g , y is the measured FT-IR functional group moles for functional group g , $EV(\%)_y$ is the variance explained in y (absorbance), and j designates each wavenumber/predictor variable. $EV(\%)_y$ is calculated as:

$$EV(\%)_{y,a,g} = 100 \frac{\sum_{j=1}^p q_{g,a,j}^2 t_{g,a,j}^T t_{g,a,j}}{\sum_{i=1}^N (y_g - \hat{y}_g)^2} \quad \text{Equation 2}$$

where t is the set of PLS scores, y is the reference moles of functional group g and \hat{y} is the FT-IR predicted moles of functional group g , and i designates the number of lab standard spectra in the calibration model for functional group g up to N .

13 Model Interpretation: Calibration and Test Set Standard Measurements

Each functional group calibration model was tested initially by applying the regression coefficients from the PLS results to the calibration set of laboratory standards (used in the calibration) and to the test set of laboratory

standards (separate from the calibration process, and used only for testing the models). The scatter plots for each functional group are shown in Figure S-13 and Figure S-14.

Coefficients of determination (R^2) were ≥ 0.97 for all calibration set laboratory standard scatter plots, and ≥ 0.93 for all test set of laboratory standard scatter plots, indicating good linearity between measured and reference moles of each functional group. No general over- or under-prediction was observed (all slopes were within 1.0 ± 0.1). Oxalic acid (teal) responses were sometimes under-predicted in the test set of laboratory standards because some of the chemical volatilized during the weighing and FT-IR analysis process. Standards with this observed trend were moved to the test set rather than calibration set of laboratory standards so that this effect would not be included in the calibration models.

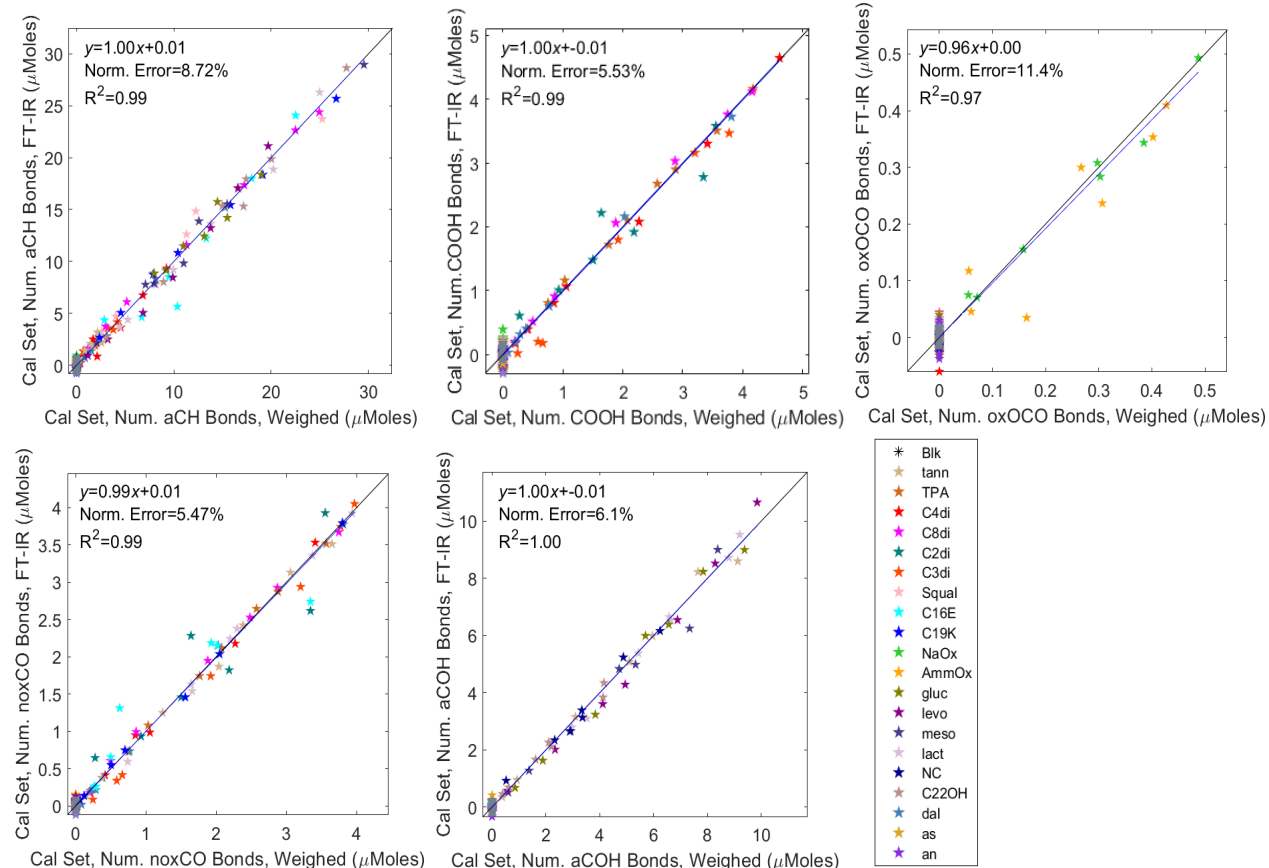


Figure S-13. Scatter plots of calibration set of laboratory standard moles. Each functional group that was calibrated is demonstrated in a separate subplot (designated in the axis titles). Note that some spread in the predicted moles was observed for interferent species (at 0 μmoles weighed along the x-axis).

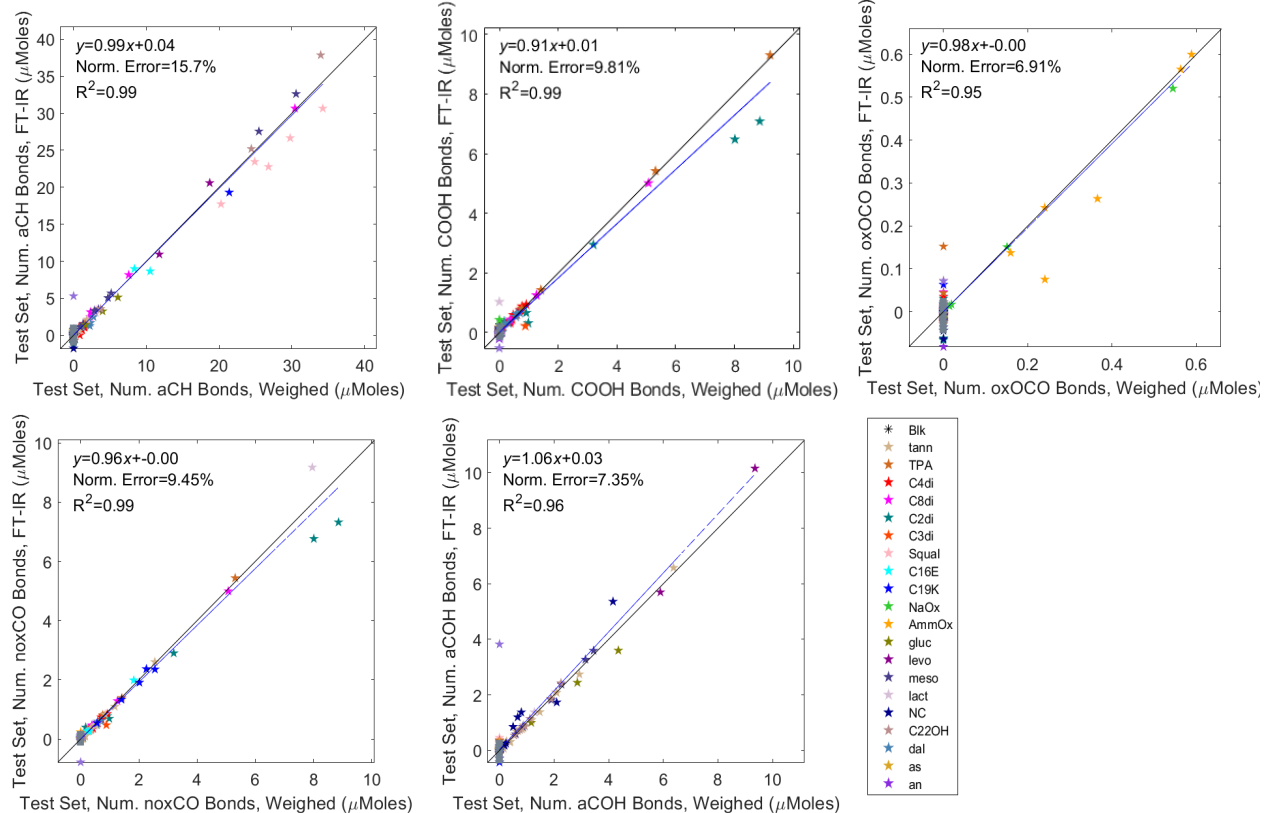


Figure S-14. Scatter plots of measured test set of laboratory standard moles. Each functional group that was calibrated is demonstrated in a separate subplot (designated in the axis titles). Note that some spread in the predicted moles was observed for interferent species (at 0 μ mole weighed along the x-axis).

14 Ambient Samples: Outlier Analysis for Silica (Dust)

Spectra containing high SEARCH network Si concentrations were identified within the dataset (as measured using X-ray fluorescence; “high” designated as $>95^{\text{th}}$ percentile within samples). An apparent mis-prediction of O/C and H/C ratios was observed for samples with S-OH stretching peaks in the FT-IR spectra (three to four sharp peaks at approx. 3750-3550 cm^{-1} ; Madejová and Komadel, 2001). Similar mis-prediction by functional group calibrations was discovered in a previous ambient sample publication due to S-OH (Reggente et al., 2018). These samples were almost exclusively collected in July, and included 54 samples total (4.4% of all samples), 51 of which were from July (18% of July samples). Removing the samples from the dataset was discussed, but because the origin of the apparent mis-prediction of O/C and H/C for these samples was complex and likely related to model regression coefficients, it was decided that the samples should be kept. Discussion of this result should be continued; collecting laboratory standards of S-OH/dust would be challenging, but could allow the models to account for dust-impacted aerosol.

15 Ambient Samples: Baseline Correction

Baseline correction of spectra for visualization was carried out using a manual smoothing splines algorithm (Kuzmiakova et al., 2016). Data in multivariate analyses were not baseline corrected, in part because of the low loading of SEARCH filters in contrast to those from the IMPROVE network (Figure S-15). The capability of baseline correction algorithms to reproducibly and accurately remove baseline features such as scattering from the filter spectra was decreased with the lesser SEARCH filter loadings.

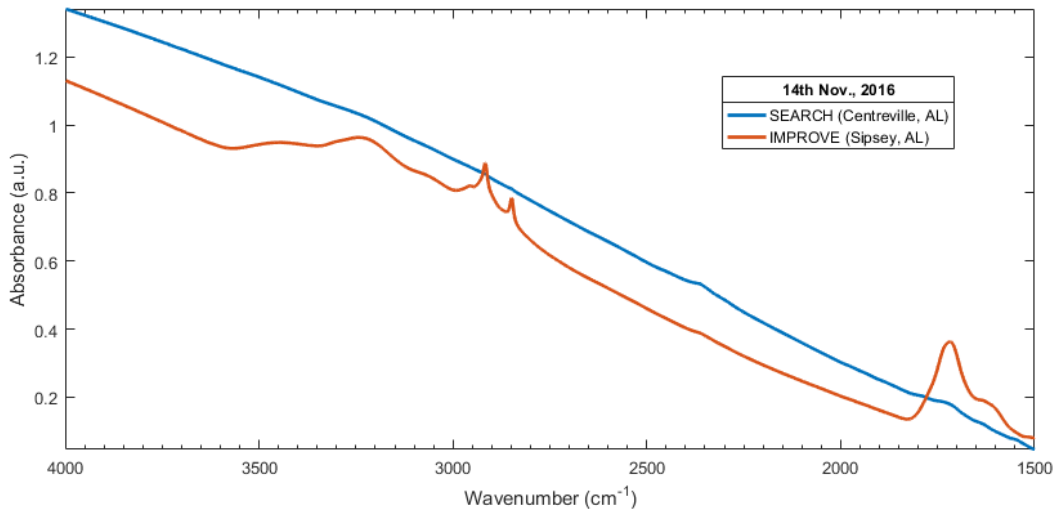


Figure S-15. Spectral examples from the IMPROVE and SEARCH networks from the 14th November, 2016. Sites are Sipsey, AL (SIPS1) in IMPROVE and Centreville, AL (CTR) in SEARCH. Note that the sites are only in the same region, and not adjacent. Spectra are raw (not baseline corrected) and truncated above 1500 cm⁻¹.

16 Ambient Samples: OM stability over time

Subsets of ambient filter samples were re-analyzed by FT-IR spectrometry, with several treatments to test the effects of FT-IR analysis and handling, long-term storage/transport and storage/transport of fresh samples. The treatments used to test these possible sources of changes/loss of aerosol material were as follows. To test FT-IR spectrometry analysis and handling, a subset of samples from all years and sites were re-analyzed within approximately one hour of the original analysis (“duplicate” analysis). To test long-term storage several years after collection, 2011 SEARCH samples were re-analyzed two years after the first analysis (2011 samples were first analyzed five years after collection, and re-analyzed seven years after collection). To test storage/transport in the first few years after collection (“fresh samples”), 2016 samples were re-analyzed after one year of storage, and again after two years of storage.

The majority of the duplicate FT-IR spectrometry measurement differences were due to slight changes in water vapor and PTFE absorption (in agreement with our previous work documenting typical differences between FT-IR spectra; Debus et al., 2018). Only minimal changes were observed for duplicate FT-IR analyses: 100% of duplicate OM concentration and ≥95% of duplicate functional group concentration biases were within sampling uncertainty (although 86% for naCO). A small median decrease in OM concentrations was observed for fresh (2016) samples,

with a greater effect after the second year of storage. For about one quarter of the fresh data, a measurable decrease in OM concentration (larger than sampling uncertainty) was observed after two years (12% of samples showed measurable decrease after one year). This suggests that fresh samples are subject to some loss of OM due to storage and handling. However, samples analyzed after five years, and again after seven years of storage showed minimal change (85% of OM and $\geq 96\%$ of functional group sample concentrations were within sampling uncertainty), suggesting equilibration of OM concentrations and composition after long-term storage of samples.

All median biases, aside from aCOH in the 2016 samples after two years, were within sampling uncertainties for each functional group, suggesting overall mostly stable measurements. The 2016 aCOH concentrations decreased ($-0.13 \mu\text{g m}^{-3}$ or -19% median bias) after two years, with $\sim 50\%$ of measurements differing by greater than the sampling uncertainty. For older (2011) samples, 71% of the aCOH values were within sampling uncertainty, indicating that aCOH concentrations were more stable. Changes in concentrations of oxOCO were variable and near zero throughout the re-analysis results. Decreases of other functional groups were -3 to -10% median bias after one year, and -5 to -17% median bias after two years for fresh (2016) samples. However, we measured the opposite trend (increases) of $+0.8\%$ to $+13\%$ after longer-term storage of (2011) samples, suggesting that these small percent differences were not meaningful.

Table S-2. Summary of median biases and the number of values within sampling uncertainty, observed after re-analysis of SEARCH ambient samples, using various treatments.

Functional Group	Duplicate Analysis			2011 Re-Analysis, Year Two		2016 Re-Analysis, Year One		2016 Re-Analysis, Year Two	
	Sampling Uncertainty, $\mu\text{g m}^{-3}$	Median Bias, $\mu\text{g m}^{-3}$	Values within $\mu\text{g m}^{-3}$	Median Bias, $\mu\text{g m}^{-3}$	Values within %	Median Bias, $\mu\text{g m}^{-3}$	Values within %	Median Bias, $\mu\text{g m}^{-3}$	Values within %
		(%)		(%)	Uncertainty, %	(%)	Uncertainty, %	(%)	Uncertainty, %
Organic Matter (OM)	0.39	-0.07 (-3%)	100	0.19 (6%)	85	-0.1 (-5%)	88	-0.3 (-11%)	72
Aliphatic Hydrocarbon (aCH)	0.15	-0.02 (-3%)	95	0.04 (3%)	81	-0.05 (-6%)	76	-0.08 (-10%)	67
Carboxylic Acids (COOH)	0.15	-0.03 (-6%)	97	0.04 (6%)	84	-0.02 (-3%)	84	-0.03 (-5%)	81
Oxalate Carbonyl (oxOCO)	0.04	-0.012 (-5%)	98	-0.001 (0.8%)	89	0.02 (9%)	84	0.02 (12%)	79
Non-Acid Carbonyl (naCO)	0.08	0.018 (9%)	86	0.008 (11%)	85	-0.02 (-10%)	74	-0.04 (-17%)	67
Alcohol (aCOH)	0.13	-0.013 (-3%)	97	0.08 (13%)	71	-0.04 (-7%)	79	-0.13 (-19%)	48

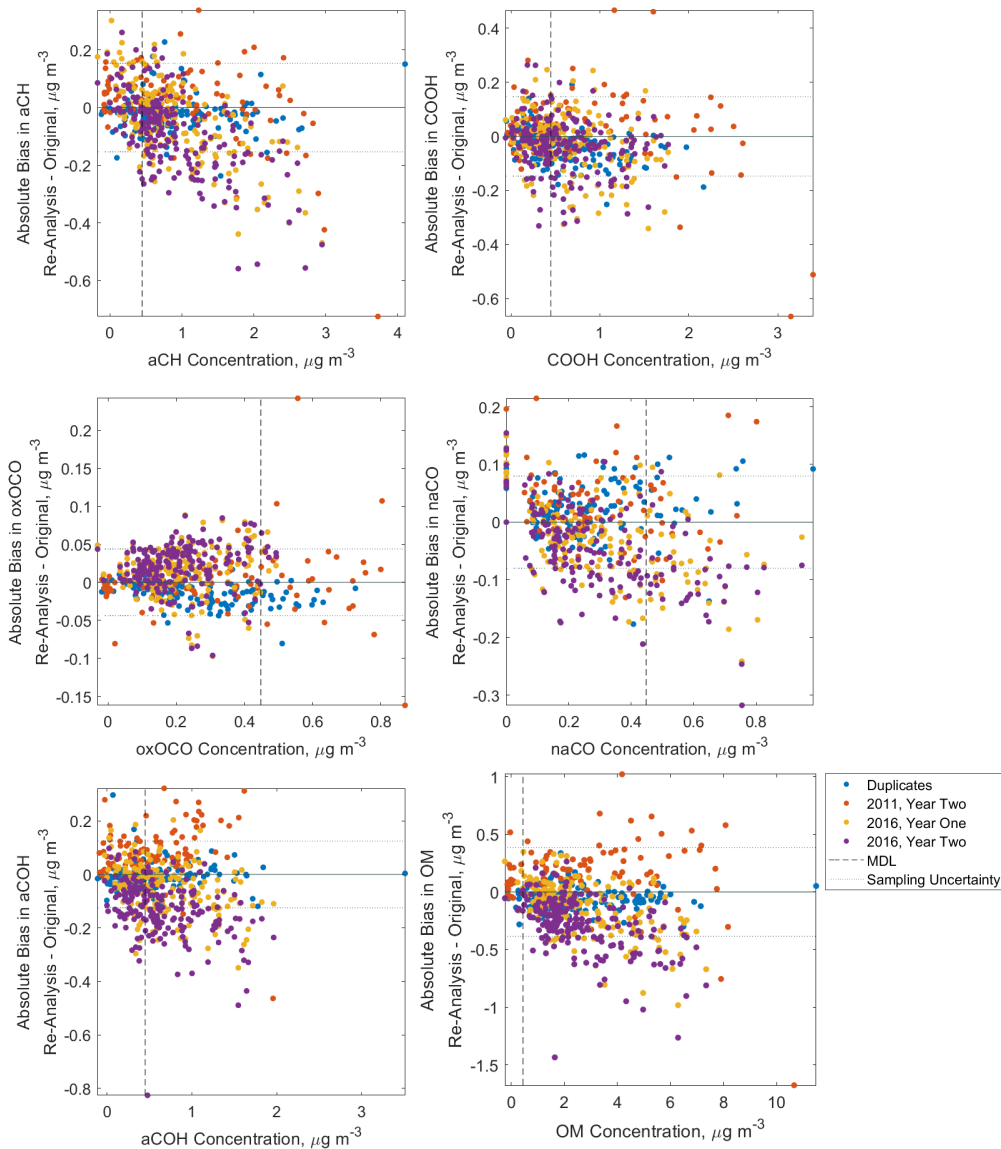


Figure S-16. Biases of functional group and OM concentrations arising after various FT-IR spectrometry re-analysis treatments. Duplicate analyses were made after approximately one hour (samples from all years and sites of data). Re-analyses of 2011 data were made after five years and seven years of sample storage to test longer-term storage. 2016 samples were re-analyzed one year and again two years after initial analysis, representing fresh samples.

17 Method Uncertainty: Collocated Atlanta Sampling Sites

Ambient samples from the collocated sampler at the Jefferson Street, Atlanta site (collocated JST/cJST) were analyzed via FT-IR spectrometry, and functional group concentrations were predicted using our calibration models. The resulting concentrations, as well as concentrations of OC and OM, were compared to those for the JST site (Figure S-17). The resulting precision gave an estimate of the error resulting from sampling the aerosol, handling

and storage, and FT-IR analysis, which is included within our bias corrected error. The magnitude of the collocated precision does not include some sources of calibration model prediction error.

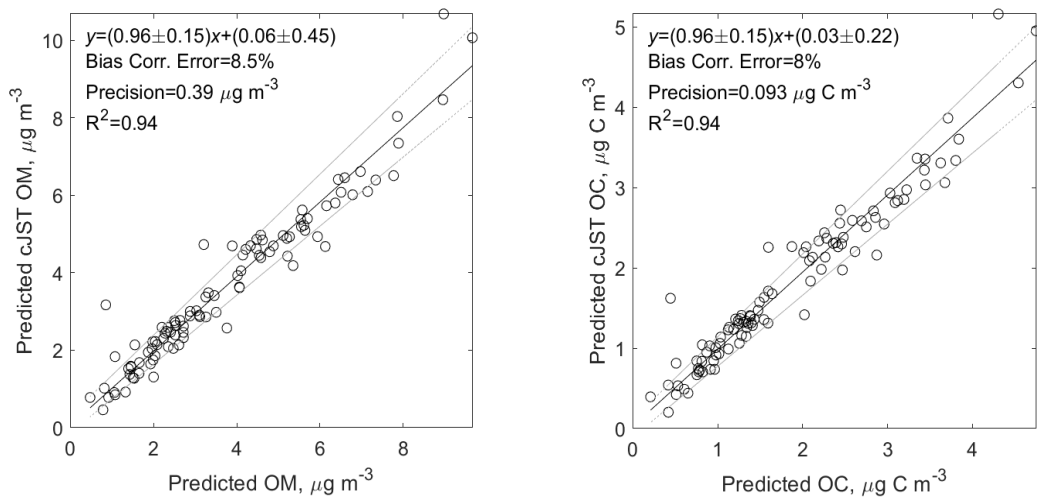


Figure S-17. Scatter plot of predicted cJST OM (left) and OC (right) concentrations versus predicted JST OM and OC concentrations. Solid lines demonstrate the slopes of the orthogonal least squares fit; confidence intervals of bootstrapped data points about the slope are shown in dashed lines. Errors reported with the slope and intercept in the regression equation are the bootstrapped confidence intervals about the slope and intercept. The precision was calculated as outlined in the methods section of the paper (also see Weakley et al., 2016).

18 Model Uncertainty: Sensitivity to Selection of Chemicals

The resilience of the model predictions to the selection of chemicals included was examined. During the construction of models for each “leave one out” case, the number of factors was allowed to vary, and chosen based on the minimum RMSECV. The uncertainty was assessed using the same relationship as in the collocated sampling uncertainty estimates, which is based on a pooled calculation (Hyslop and White, 2008, 2009). The predicted concentrations from the “base case”, which included every chemical in the full list, were used as the “reference” predictions. The calculated uncertainties, expressed as percentages of the concentrations of each functional group, OM and OC, are summarized in Figure S-18.

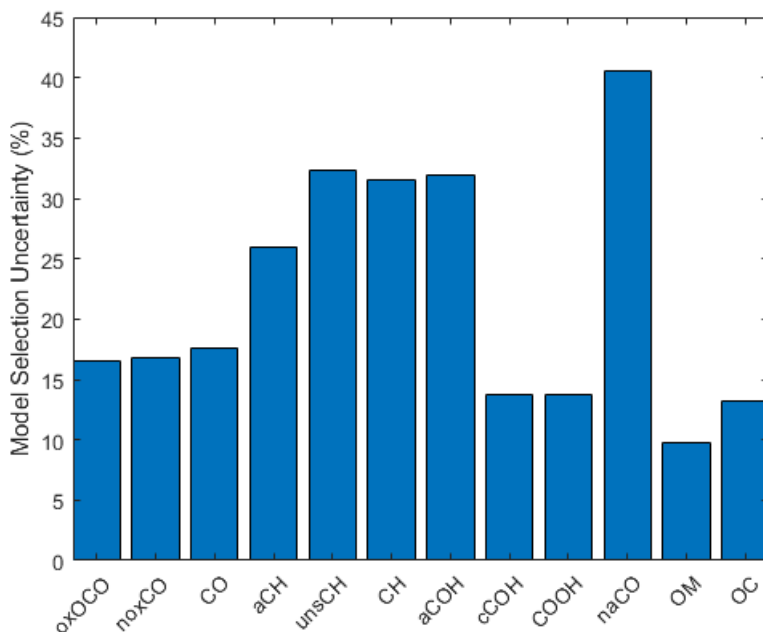


Figure S-18. Uncertainties calculated as the difference in model predictions between the model set with all chemicals included and each chemical left out (mean of all models with one chemical left out, as in Hyslop and White, 2008, is reported for each functional group).

The uncertainty for each functional group was on the same order of magnitude as that calculated for the collocated sampling sites (14-32% for the functional groups reported and used in the final model set: aCH, COOH, oxOCO, naCO, and aCOH). The uncertainty was higher (~40%) for naCO than for the other functional groups because of the small (sometimes null) contribution from this group; it was partitioned from the linear relationship between COOH and noxOCO, rather than being obtained by calibration from the model set. Uncertainties associated with OM and OC concentrations were low (10 and 13%, respectively), likely because of the overall greater concentrations of these aggregated variables, and because each chemical only affected some of the functional groups, and not the entire mass making up the OM and OC concentrations.

In addition to the uncertainty calculated over all chemical removal cases, and all samples, the individual cases in which each chemical was removed from the models, and the ambient sample functional group concentrations were re-measured. The results demonstrated that functional groups with low concentrations were related to greater chemical selection uncertainty: naCO was highly uncertain given the removal of nearly any chemical (removing D-alanine, sodium oxalate, glucono-delta-lactone, and nonadecanone each introduced more than 50% uncertainty). The resilience of some functional groups to chemical selection was also related to the number of chemicals in a given functional group model: oxOCO, for example, was modeled with only two chemicals, such that removing either sodium or ammonium oxalate from the model resulted in added uncertainty (30 and 40%, respectively, compared to ~3-15% for most other chemicals; Figure S-19). This observation was likely enhanced by the spectral dissimilarity of ammonium and sodium oxalates, and the spectral overlap within multiple regions of these standards with the other functional group standards. This observation points to two aspects of model development that should continue to be considered in future calibrations. The first is that including multiple chemicals in each functional group model

adds robustness. The second is that quantifying sub-functional groups separately allows models to capture variability in composition between samples more adeptly (as more specific spectral information is provided to a model, such as oxOCO response separate from other carbonyl response, the model will more precisely describe the functional group). In contrast, the model of COOH (Figure S-20) contained information from many more chemicals (six), such that removing any given chemical containing (or interfering with the absorption region of) a carboxylic acid functional group was less influential than in the case of oxOCO (mostly ~5-20% uncertainty, with squalene 3% and terephthalic acid or TPA 32%; Figure S-19). Thus, models are more robust to mis-specification of model parameters (including missing chemicals) when several, spectrally similar (but not equivalent) chemicals are included.

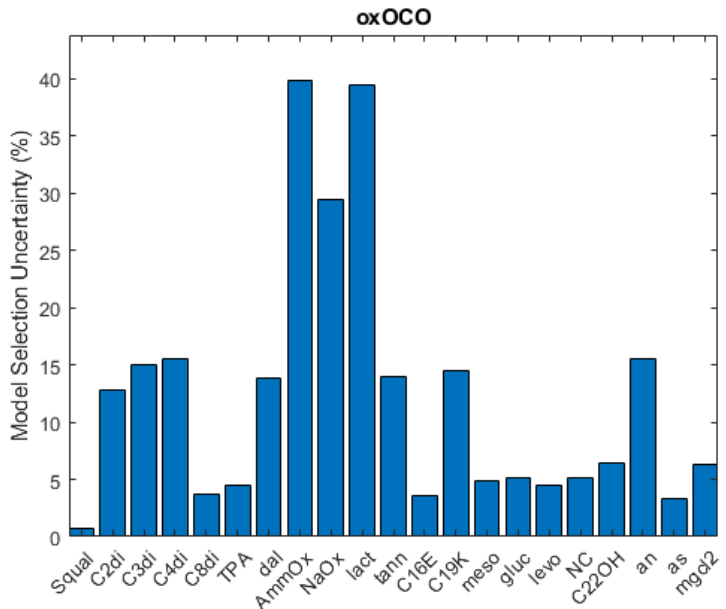


Figure S-19. Model selection uncertainty introduced by leaving out a chemical (x-axis) for aCOH.

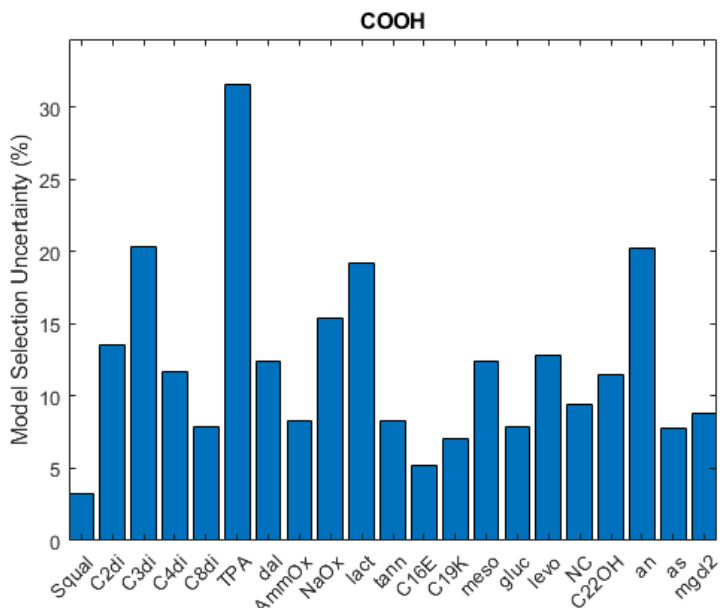


Figure S-20. Model selection uncertainty introduced by leaving out a chemical (x-axis) for COOH.

A regression between the predicted functional group FT-IR OM concentrations in ambient samples without (y-axis) and with (x-axis) a particular chemical in the calibration models in general demonstrated agreement: tannic acid, oxalic acid, succinic acid, and suberic acid removal from the calibration models resulted in a scatter plot slope of 0.96-1.06. However, the OM concentration predictions were less resilient to the removal of inorganic salt interferents: removing ammonium sulfate and ammonium nitrate resulted in a scatter plot slope (predicted functional group FT-IR OM without vs. with these salts) of 0.82 (Figure S-21).

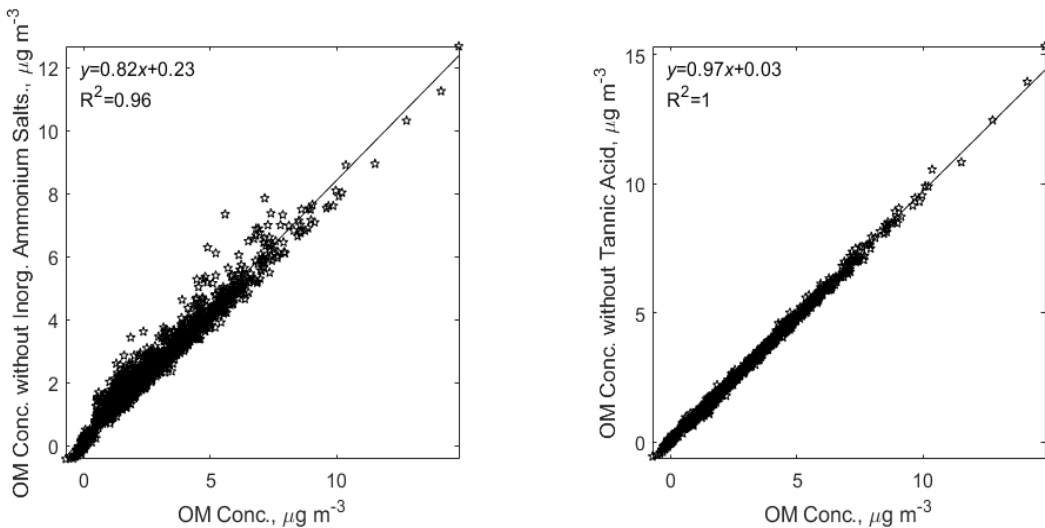


Figure S-21. OM concentrations contrasted between model with all chemicals, and after leaving ammonium sulfate and ammonium nitrate (left) and tannic acid (right) out of the calibration models.

Thus, although the model included a variety of organic species substantial enough to describe ambient aerosol spectral variance even without some of the most abundant species (e.g., tannic and oxalic acids), including abundant inorganic salts was essential to predicting OM concentrations successfully.

References

- Andersson, M.: A comparison of nine PLS1 algorithms, *J. Chemom.*, 23(10), 518–529, doi:10.1002/cem.1248, 2009.
- Bahadur, R., Uplinger, T., Cliff, S. S., Millet, D. B., Goldstein, A., Bates, T. S., Russell, L. M., Sive, B. C., Cliff, S. S., Millet, D. B., Goldstein, A. and Bates, T. S.: Phenol groups in northeastern U.S. submicrometer aerosol particles produced from seawater sources, *Environ. Sci. Technol.*, 44(7), 2542–2548, doi:10.1021/es9032277, 2010.
- Barros, T. C., Yunes, S., Menegon, G., Nome, F., Chaimovich, H., Politi, M. J., Dias, L. G. and Cuccovia, I. M.: Hydrolysis of 1,8- and 2,3-naphthalic anhydrides and the mechanism of cyclization of 1,8-naphthalic acid in aqueous solutionsThe IUPAC name for naphthalic acid is naphthalenedicarboxylic acid.Electronic supplementary information (ESI) available: tables con, *J. Chem. Soc., Perkin Trans.*, (12), 2342–2350, doi:10.1039/b104148g, 2001.
- Chalmers, J. M.: Anomalies, Artifacts and Common Errors in Using Vibrational Spectroscopy Techniques, in *Handbook of Vibrational Spectroscopy*, edited by J. M. Chalmers and P. R. Griffiths, pp. 2327–2347, John Wiley & Sons Ltd., Chichester., 2002.
- Chong, I. G. and Jun, C. H.: Performance of some variable selection methods when multicollinearity is present, *Chemom. Intell. Lab. Syst.*, 78(1), 103–112, doi:10.1016/j.chemolab.2004.12.011, 2005.
- Cziczo, D. J. and Abbatt, J. P. D.: Infrared Observations of the Response of NaCl, MgCl₂, NH₄HSO₄, and NH₄NO₃ Aerosols to Changes in Relative Humidity from 298 to 238 K, *J. Phys. Chem. A*, 104(10), 2038–2047, doi:10.1021/jp9931408, 2000.

- Dabek-Zlotorzynska, E., Dann, T. F., Kalyani Martinelango, P., Celo, V., Brook, J. R., Mathieu, D., Ding, L. and Austin, C. C.: Canadian National Air Pollution Surveillance (NAPS) PM_{2.5} speciation program: Methodology and PM_{2.5} chemical composition for the years 2003–2008, *Atmos. Environ.*, 45(3), 673–686, doi:10.1016/j.atmosenv.2010.10.024, 2011.
- Davey, R. J., Dent, G., Mughal, R. K. and Parveen, S.: Concerning the relationship between structural and growth synthons in crystal nucleation: Solution and crystal chemistry of carboxylic acids as revealed through IR spectroscopy, *Cryst. Growth Des.*, 6(8), 1788–1796, doi:10.1021/cg060058a, 2006.
- Debus, B., Takahama, S., Weakley, A. T., Seibert, K. and Dillner, A. M.: Long term strategy for assessing carbonaceous particulate matter concentrations from multiple FT-IR instruments: influence of spectral dissimilarities on multivariate calibration performance, *Appl. Spectrosc.*, 2018.
- Frossard, A. A. and Russell, L. M.: Removal of sea salt hydrate water from seawater-derived samples by dehydration, *Environ. Sci. Technol.*, 46(24), 13326–13333, doi:10.1021/es3032083, 2012.
- Hyslop, N. P. and White, W. H.: An evaluation of interagency monitoring of protected visual environments (IMPROVE) collocated precision and uncertainty estimates, *Atmos. Environ.*, 42(11), 2691–2705, doi:10.1016/j.atmosenv.2007.06.053, 2008.
- Hyslop, N. P. and White, W. H.: Estimating precision using duplicate measurements, *J. Air Waste Manag. Assoc.*, 59(9), 1032–1039, doi:10.3155/1047-3289.59.9.1032, 2009.
- Kuzmiakova, A., Dillner, A. M. and Takahama, S.: An automated baseline correction protocol for infrared spectra of atmospheric aerosols collected on polytetrafluoroethylene (Teflon) filters, *Atmos. Meas. Tech.*, 9(6), 2615–2631, doi:10.5194/amt-9-2615-2016, 2016.
- Ledesma, S., Ruiz, J. and Garcia, G.: Simulated Annealing Evolution, in *Simulated Annealing: Advances, Applications and Hybridizations*, edited by M. S. G. Tsuzuki, InTech., 2012.
- Li, B. B., Morris, J. and Martin, E. B.: Model selection for partial least squares regression, *Chemom. Intell. Lab. Syst.*, 64(1), 79–89, 2002.
- Liang, C. Y. and Krimm, S.: Infrared Spectra of High Polymers . III . Polytetrafluoroethylene and Polychlorotrifluoroethylene Infrared Spectra of High Polymers . III . Polytetrafluoroethylene, *J. Chem. Phys.*, 25(3), 563–571, doi:10.1063/1.1742964, 1996.
- Madejová, J. and Komadel, P.: Basline studies of the clay minerals society source clays: Infrared methods, *Clay Clay Miner.*, 49(5), 410–432, doi:10.1346/CCMN.2001.0490508, 2001.
- Maroń, M. K., Takahashi, K., Shoemaker, R. K. and Vaida, V.: Hydration of pyruvic acid to its geminal-diol, 2,2-dihydroxypropanoic acid, in a water-restricted environment, *Chem. Phys. Lett.*, 513(4–6), 184–190, doi:10.1016/j.cplett.2011.07.090, 2011.
- Mayo, D. W., Miller, F. A. and Robert W, H.: Course Notes on the Interpretation of Infrared and Raman Spectra, John Wiley & Sons, Inc., Hoboken, New Jersey., 2003.
- Naes, T., Isaksson, T., Fearn, T. and Davies, T.: A User-Friendly Guide to Multivariate Calibration and Classification, NIR Publications, Chichester., 2002.

Reggente, M., Dillner, A. M. and Takahama, S.: Analysis of functional groups in atmospheric aerosols by infrared spectroscopy: functional group quantification in US measurement networks, Submitted, doi:10.1016/j.atmosenv.2013.12.034, 2018.

Solomons, T. W. G. and Fryhle, C. B.: Organic Chemistry, 8th ed., John Wiley & Sons, Hoboken, New Jersey., 2004.

Takahama, S. and Dillner, A. M.: Model selection for partial least squares calibration and implications for analysis of atmospheric organic aerosol samples with mid-infrared spectroscopy, *J. Chemom.*, 29(12), 659–668, doi:10.1002/cem.2761, 2015.

Takahama, S., Johnson, A. and Russell, L. M.: Quantification of Carboxylic and Carbonyl Functional Groups in Organic Aerosol Infrared Absorbance Spectra, *Aerosol Sci. Technol.*, 47(3), 310–325, doi:10.1080/02786826.2012.752065, 2013.

van der Voet, H.: Comparing the predictive accuracy of models using a simple randomization test, *Chemom. Intell. Lab. Syst.*, 25(2), 313–323, doi:10.1016/0169-7439(94)85050-X, 1994.

Weakley, A. T., Takahama, S. and Dillner, A. M.: Ambient aerosol composition by infrared spectroscopy and partial least-squares in the chemical speciation network: Organic carbon with functional group identification, *Aerosol Sci. Technol.*, 50(10), 1096–1114, doi:10.1080/02786826.2016.1217389, 2016.